J. Fluid Mech. (1976), *vol.* 76, *part* 1, *pp.* 1–15
Printed in Great Britain

Axisymmetric laminar wake behind a slender body of revolution

By FRANCIS R. HAMA AND LEIGH F. PETERSON

Department of Aerospace and Mechanical Sciences, Princeton University, Princeton, New Jersey 08540

(Received 29 July 1975)

At the body-diameter Reynolds number 2000, the axisymmetric wake behind a slender streamlined body of revolution remained laminar without any indication of breakup far beyond the five-body-lengths test section. The mean-velocity profiles were measured with close spacings in order to obtain experimental information on the transient process from boundary layer to fully developed wake. A semi-empirical theory was developed to describe the flow-field characteristics.

1. Introduction

Flow behaviour in the transient regime as a body boundary layer leaves from the trailing edge and eventually attains an asymptotic similarity is an interesting fundamental fluid-dynamic problem, and some theoretical investigations have been carried out already. Goldstein (1930) was concerned with the development of the mean-velocity profiles immediately behind the trailing edge of an infinitely thin flat plate. Starting from the Blasius solution at the trailing edge, he expanded the stream function in a power series in essentially the downstream distance and obtained the first three terms. Tollmien (1931), on the other hand, obtained the far-wake asymptotic similarity solution. Goldstein (1933) was able to determine the second approximation to the Tollmien solution. The second approximation was then matched to the near-wake solution by an adjustment of the origin of the downstream co-ordinate in the asymptotic solution, in order to account for the finite boundary-layer thickness at the trailing edge. It is worth noting here that Goldstein encountered a mathematical difficulty in obtaining the third approximation. Stewartson (1957) removed the difficulty by including a logarithm in the series expansion.

These theoretical investigations were the two-dimensional problems of the wake behind a flat plate. Goldstein (1933) compared his theoretical results with the experimental results obtained by Fage & Falkner. Whereas the two agreed well in the region immediately behind the trailing edge, the experimentally obtained centre-line velocity as well as the lateral extent of the wake were already much larger than the theoretical predictions at the downstream distance of only half the plate length. The discrepancies were attributed to flow instability. Sato & Kuriki (1961) made a detailed experimental investigation of the instability

phenomena and demonstrated that the prompt deviation of the flow field from the Goldstein solution within such a short distance as one-tenth of the plate length was indeed due to the instability, which resulted in the formation of Kármán vortex streets and eventual transition to turbulence. More recent work on the same subject by Mattingly & Criminale (1972) included the mean-velocity profiles, which showed a grossly different initial behaviour of the centre-line velocity in the near-wake region. The discrepancy is inexplicable and suspected to be due to the characteristics of the hot-film anemometer, which might have been different from the assumed linear properties. In any event, the steady two-dimensional theories could not be experimentally substantiated owing to the inherent instability, which quickly destroyed the steady flow.

We have been engaged in an experimental investigation of the instability and transition of the axisymmetric wake behind a slender streamlined body of revolution with a pointed trailing tip which was as sharp as a pin. When the alignment of the body was critically accomplished and the Reynolds number was approximately 2000, dye inserted upstream of the body was swept as far downstream as ten body lengths without any indication of unsteadiness or breakdown. This behaviour was quite contrary to that of the two-dimensional wake, which was observed to form Kármán vortices quite promptly at a comparable body-length Reynolds number. The axisymmetric wake provided us with an excellent opportunity to explore experimentally the behaviour of the steady velocity field in the transient process from the boundary layer to the wake. This paper presents primarily the results of such an experiment. On the basis of the experimental information thus obtained, semi-empirical analyses were developed in order to describe the general flow characteristics. Before presenting the experimental results and discussions, however, a brief review of the existing theories of the steady axisymmetric wake will be given.

2. Theoretical review

The basic equations for the axisymmetric wake are

$$U\frac{\partial U}{\partial X}+V\frac{\partial U}{\partial Y}=\frac{\nu}{Y}\frac{\partial}{\partial Y}\left(Y\frac{\partial U}{\partial Y}\right)$$

and

$$\frac{\partial U}{\partial X}+\frac{\partial V}{\partial Y}+\frac{V}{Y}=0,$$

in which U and V are dimensional velocity components in the longitudinal and radial directions X and Y respectively. When the velocity components and the co-ordinates are normalized by the use of the free-stream velocity U_0 and a characteristic length l to give

$$u=U/U_0,\quad v=(V/U_0)(U_0 l/\nu)^{\frac{1}{2}},\quad x=X/l,\quad y=(Y/l)(U_0 l/\nu)^{\frac{1}{2}},$$

the governing equations become

$$u\frac{\partial u}{\partial x}+v\frac{\partial u}{\partial y}=\frac{1}{y}\frac{\partial}{\partial y}\left(y\frac{\partial u}{\partial y}\right), \tag{1}$$

$$\frac{\partial u}{\partial x}+\frac{\partial v}{\partial y}+\frac{v}{y}=0. \tag{2}$$

In terms of the velocity defect $w = 1-u$, we obtain

$$(1-w)\frac{\partial w}{\partial x}+v\frac{\partial w}{\partial y}=\frac{1}{y}\frac{\partial}{\partial y}\left(y\frac{\partial w}{\partial y}\right), \tag{3}$$

$$\frac{\partial w}{\partial x}=\frac{\partial v}{\partial y}+\frac{v}{y}. \tag{4}$$

The asymptotic far-wake solution w_1, which corresponds to the Tollmien solution for the two-dimensional wake, can be obtained after linearizing (3) under the approximation $w_1 \ll 1$, which yields

$$\frac{\partial w_1}{\partial x}=\frac{1}{y}\frac{\partial}{\partial y}\left(y\frac{\partial w_1}{\partial y}\right), \tag{5}$$

and is given by

$$w_1 = x^{-1}f_1(\eta) = A\,x^{-1}\exp\left(-\tfrac{1}{2}\eta^2\right), \tag{6}$$

where

$$\eta = \frac{y}{(2x)^{\frac{1}{2}}} = Y\left(\frac{U_0}{2\nu X}\right)^{\frac{1}{2}} \tag{7}$$

(cf. Rosenhead 1963, p. 455). The coefficient A is related to the drag on the body

$$D = \rho\int_0^\infty U(U_0-U)\,2\pi Y\,dY \approx 2\pi\mu U_0\,l\int_0^\infty w_1\,y\,dy$$

by

$$A = D/4\pi\mu U_0\,l. \tag{8}$$

Substituting w_1 as given by (6) into the continuity equation (4), we obtain

$$v_1 = -\frac{2^{\frac{1}{2}}A}{x^{\frac{3}{2}}}\tfrac{1}{2}\eta\exp\left(-\tfrac{1}{2}\eta^2\right). \tag{9}$$

To this order of approximation, at which w_1^2 is omitted, the displacement area

$$\Delta = \int_0^\infty\left(1-\frac{U}{U_0}\right)2\pi Y\,dY \tag{10}$$

and the momentum (loss) area

$$\Theta = \int_0^\infty\frac{U}{U_0}\left(1-\frac{U}{U_0}\right)2\pi Y\,dY \tag{11}$$

are identical.

Now, if the second approximation to the asymptotic similarity solution (6) is sought in such a form as

$$w_2 = 1-u-w_1 = x^{-2}f_2(\eta),$$

one faces the same mathematical difficulty as in the third approximation attempted by Goldstein (1933) for the two-dimensional wake. Following the guideline used by Stewartson (1957), Berger (1968) successfully obtained the second approximation for the axisymmetric case by including an additional term involving a logarithm, i.e. by setting

$$w_2 = x^{-2}f_2(\eta)+x^{-2}\ln x\,f_2^*(\eta). \tag{12}$$

When (12) is substituted into the equation for w_2, i.e.

$$\frac{1}{y}\frac{\partial}{\partial y}\left(y\frac{\partial w_2}{\partial y}\right)-\frac{\partial w_2}{\partial x}=v_1\frac{\partial w_1}{\partial y}-w_1\frac{\partial w_1}{\partial x}, \tag{13}$$

we obtain

$$\tfrac{1}{2}x^{-3}[\eta^{-1}(f_2'+\eta f_2'')+4f_2+\eta f_2']+\tfrac{1}{2}x^{-3}\ln x\,[\eta^{-1}(f_2^{*\prime}+\eta f_2^{*\prime\prime})+4f_2^*+\eta f_2^{*\prime}]-x^{-3}f_2^* = A^2x^{-3}\exp(-\eta^2), \tag{14}$$

the right-hand side arising from the first approximation (6) and (9). For (14) to be applicable at any x, the following two equations must be satisfied:

$$\eta f_2^{*\prime\prime}+(1+\eta^2)f_2^{*\prime}+4\eta f_2^*=0, \tag{15}$$

$$\eta f_2''+(1+\eta^2)f_2'+4\eta f_2=2\eta f_2^*+2A^2\eta\exp(-\eta^2). \tag{16}$$

The solutions of these equations satisfying appropriate boundary conditions are

$$f_2^*=-\tfrac{1}{4}A^2(1-\zeta)e^{-\zeta}, \tag{17}$$

$$f_2=\tfrac{1}{4}A^2\left[2e^{-\zeta}+e^{-2\zeta}+(1-\zeta)e^{-\zeta}\int_0^\zeta\frac{1-e^{-t}}{t}dt\right]+C(1-\zeta)e^{-\zeta}, \tag{18}$$

where

$$\zeta=\tfrac{1}{2}\eta^2, \tag{19}$$

for brevity, and C is an undetermined integration constant. To this order of approximation the centre-line velocity defect is therefore given by

$$1-u(x,0)=Ax^{-1}-\tfrac{1}{4}A^2x^{-2}\ln x+\tfrac{3}{4}A^2x^{-2}+Cx^{-2}. \tag{20}$$

While the far-wake solution has thus been developed to an extent comparable to the two-dimensional case, the near-wake problem is rather difficult to treat. The difficulty in fact lies in our inability to predict properly the boundary-layer characteristics over a body of revolution whose diameter reduces to zero towards a sharp trailing tip. The shear layer in such a regime appears to behave quite differently from that due to a conventional boundary layer, as observed by Patel, Nakayama & Damian (1974) with a turbulent boundary layer. Probably because of the lack of such knowledge, Viviand & Berger (1965) attempted a near-wake solution starting with the asymptotic logarithmic profile obtained by Glauert & Lighthill (1955) for the thick axisymmetric boundary layer along a circular rod of constant radius. Since the boundary-layer characteristics at the trailing tip in the present problem are not those of Glauert & Lighthill, the Viviand–Berger solution is not applicable. Under such circumstances, we have to accept whatever mean-velocity profile we obtain at the trailing tip as our initial condition, on which ensuing flow development depends.

3. Experiment

The experiment was carried out in a recirculating water channel 2 ft wide, 1½ ft deep and 50 ft long in the Hydrodynamics Laboratory, Princeton University. Initially the channel was designed as a constant cross-section tilting flume and was of poor flow quality, but its turbulence level was reduced to approximately

0·1 % by the insertion of a series of fine-mesh screens and small-bore honeycombs (Mattingly & Criminale 1972) and the mean-flow profile was fairly uniform. The water was recirculated by an axial pump which was driven by a $7\frac{1}{2}$ h.p. motor through a variable-speed hydraulic coupling.

A bypass loop was provided to treat the water for reliable operation of a hot-film anemometer, as described in detail by Baily (1972). First, deaeration was essential to avoid the formation of air bubbles on the probe (Morrow & Kline 1971), and was accomplished by the application of cavitation and a vacuum pump. Second, solid particles suspended in the water were removed by two-stage Filtrine 'B' type filters, which reduced the particle size to 60–80 μm, and by a 0·3 μm Pall Trincor filter. The replacement of our original, metal honeycombs by Hexcel nylon fibre/phenolic resin honeycombs turned out to be the final key improvement, resulting in consistent and completely reproducible operation of the hot-film probe thereafter.

The wake to be studied was created by an axisymmetric body of length 12 in. and diameter 0·72 in. whose meridian shape was an NACA 0006 profile. The body was supported from above by four 0·002 in. tungsten wires each inclined 45° either forwards or backwards. In addition, two wires were attached to the lower side of the body and connected to weights. The body was mounted by means of a fine-adjustment suspension mechanism in an inner channel test section, which was made of $\frac{1}{2}$ in. Plexiglas plate and was 8 ft long, 23 in. wide and 13 in. deep. The inner channel not only separated the test section from the boundary layers on the side walls and the bottom of the flume, but also provided additional capability of fine alignment of the body. Indeed, this much provision for critical alignment became quite useful because misalignments of the order of 1′ resulted in detectable asymmetry in the mean-velocity profile in the wake, which, in turn, caused considerable variation in the stability characteristics. The wakes of the suspension wires could be detected in their close proximity, but were promptly dispersed and had no influence on the main wake of the body. The body was found by a laser beam reflecting from its surface to be absolutely stationary, without any indication of sway or oscillation.

Mean-velocity measurements were made by Thermo-Systems model 1050A constant-temperature anemometer system with a model 1051-2 digital read-out. The sensor was model 1210–20W, which is of hot-wire type and has a quartz-coated hot-film probe 0·002 in. in diameter with a sensing element of length 0·04 in. The probe was calibrated in a small towing tank, 4 in. × 4 in. and 8 ft long, using the same water as in the main channel. The hot-film probe was mounted on a traversing mechanism, which enabled us to locate it within 0·001 in. accuracy in both the horizontal and the vertical direction in a plane normal to the free-stream direction. The traversing mechanism was moved manually in the flow direction within the accuracy of a common rule, say $\frac{1}{32}$ in. The probe support was L-shaped and was placed along and perpendicular to the flow direction. The vertical portion of the L-shaped support is protected from the flow by a sheath of larger diameter to alleviate the probe vibration due to the vortex shedding from the support. The sensing element was oriented normal to the flow and was always perpendicular to the radius from the wake axis. When this experiment was con-

ducted, our laboratory was not heated owing to the energy crisis and the water temperature was 14·0–14·7 °C. The free-stream velocity U_0 was maintained at approximately 5 in./s, so that the Reynolds number based upon the body diameter was 2000 throughout the experiment. The flow of the dye inserted indicated smooth rectilinear flow patterns in the wake as well as on the body without any separation or disturbance. Since the displacement area of the wake amounted to less than 0·05% of the cross-sectional area, the blocking effect was negligible and the static pressure was presumed to be constant throughout the wake. Further experimental details are described in the second author's thesis (Peterson 1975), which is concerned with the instability and transition at a Reynolds number higher than that in the present experiment.

4. Results and discussion

Described in the following are the results of the mean-velocity profile surveys conducted at x = 0, 0·0625, 0·125, 0·25, 0·375, 0·5, 0·75, 1·0, 1·25, 1·5, 2·0, 2·5, 3·0, 3·5, 4·0 and 5·0, the characteristic length l being the body length. Before each survey, the symmetry was checked, both in the vertical and in the horizontal plane, the minimum-velocity point was located and then the mean-velocity profile was determined in the horizontal plane containing the minimum-velocity point.

Figure 1 shows the velocity profile at the trailing tip, the two symbols indicating measurements taken on oppoiste sides of the minimum-velocity point. The tendency towards a finite value near the axis is due to the fact that the traverse was actually made approximately $\frac{1}{16}$ in. behind the tip and to the finite length of the hot-film sensing element. An estimate shows that the correction needed for the finite element length is probably negligible at most other measuring locations. The ordinate of the figure is the conventional Blasius co-ordinate, and the curve is the Blasius flat-plate profile augmented to twice the thickness. Contrary to the case of the axisymmetric boundary layer along a constant-radius cylinder, the boundary layer at the trailing tip of a slender axisymmetric body is in fact much thicker than that on a two-dimensional flat plate of a comparable length. Since no measurements of the body boundary layer were actually made, detailed discussion of its behaviour is outside the scope of the present paper. It appears to behave over the rear portion of the body such that, whereas the outer part of the boundary layer is merely swept downstream nearly parallel to the free stream, the inner portion somehow adjusts itself to the decreasing body size. Under such circumstances, it is not difficult to imagine that the shear layer behaves quite differently from that due to a planar boundary layer.

The initial development of the mean-velocity profile immediately behind the trailing tip is shown in figure 2. The outer part of the wake does not seem to change at all, while the central portion around the wake axis is accelerated quite rapidly. The variation of the centre-line velocity u_c with downstream distance x is given in figure 3, where it is compared with Goldstein's two-dimensional theory (1933). The Goldstein theory predicts an $x^{\frac{1}{3}}$ law in the near wake up to approximately x = 0·1. The present results follow an $x^{\frac{1}{2}}$ dependence as far downstream as x = 2.

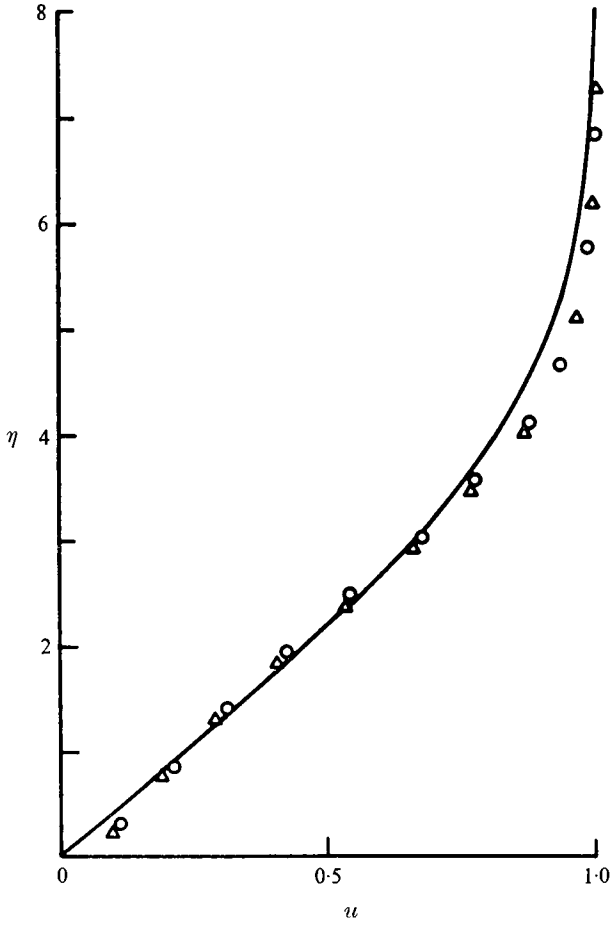

FIGURE 1. Velocity profile at trailing tip of the body. ———, Blasius profile with ordinate augmented by a factor of 2.

The $x^{\frac{1}{3}}$ dependence of the centre-line velocity thus demonstrated in the very near region can be easily assessed by a simple procedure. The velocity profiles near the axis can be quite well approximated by hyperbolas

$$u = (u_c^2 + c^2 y^2)^{\frac{1}{2}}, \tag{21}$$

in which u_c is the non-dimensional centre-line velocity and is a function of x, and c is assumed to be a constant related to the velocity gradient at $x = 0, y = 0$ by

$$c = \left(\frac{U_0 l}{\nu}\right)^{-\frac{1}{2}} \left[\frac{\partial(U/U_0)}{\partial(Y/l)}\right]_{x,\, y=0} \tag{22}$$

When the approximate velocity profile (21) is substituted into (1) and (2) and the limit $y \to 0$ is taken, we obtain an equation for u_c:

$$u_c \, du_c/dx = 2c^2/u_c,$$

whose solution is

$$u_c = (6c^2 x)^{\frac{1}{3}}. \tag{23}$$

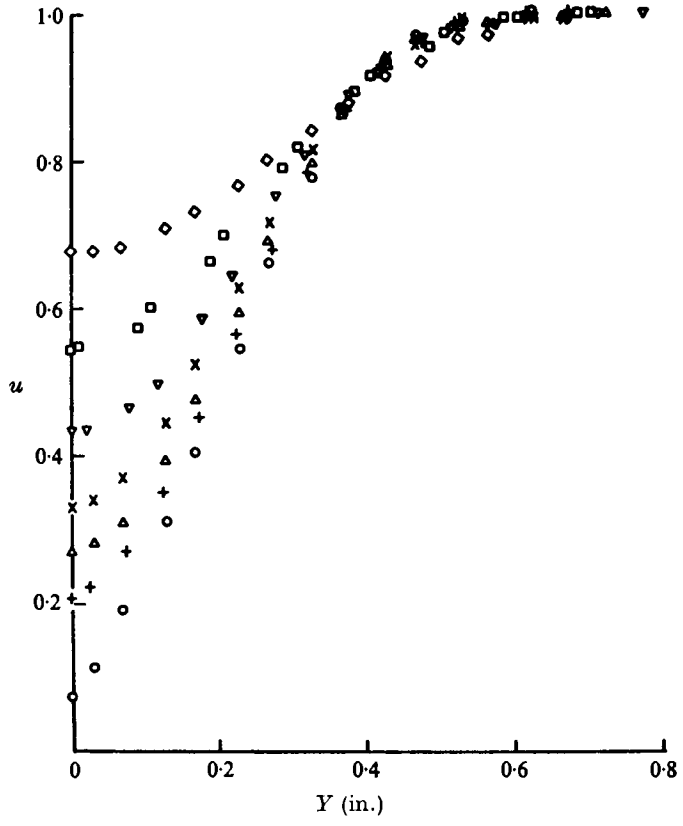

FIGURE 2. Initial development of velocity profile. ○, $x = 0$; +, $x = 0{\cdot}0625$; △, $x = 0{\cdot}125$; ×, $x = 0{\cdot}25$; ▽, $x = 0{\cdot}5$; □, $x = 1$; ◇, $x = 2$.

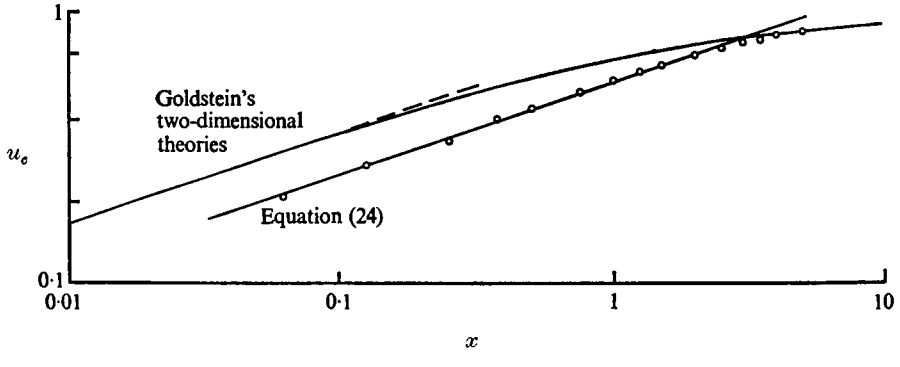

FIGURE 3. Centre-line velocity *vs.* downstream distance. ○, present experimental data.

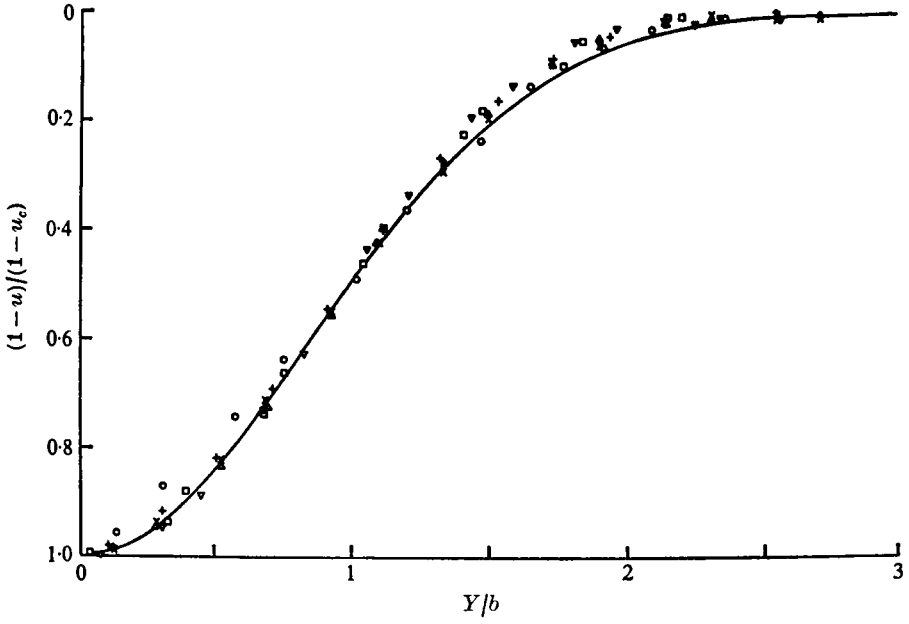

FIGURE 4. Non-dimensional velocity defect *vs.* normalized radial co-ordinate. For symbols see figure 2; ———, equation (27).

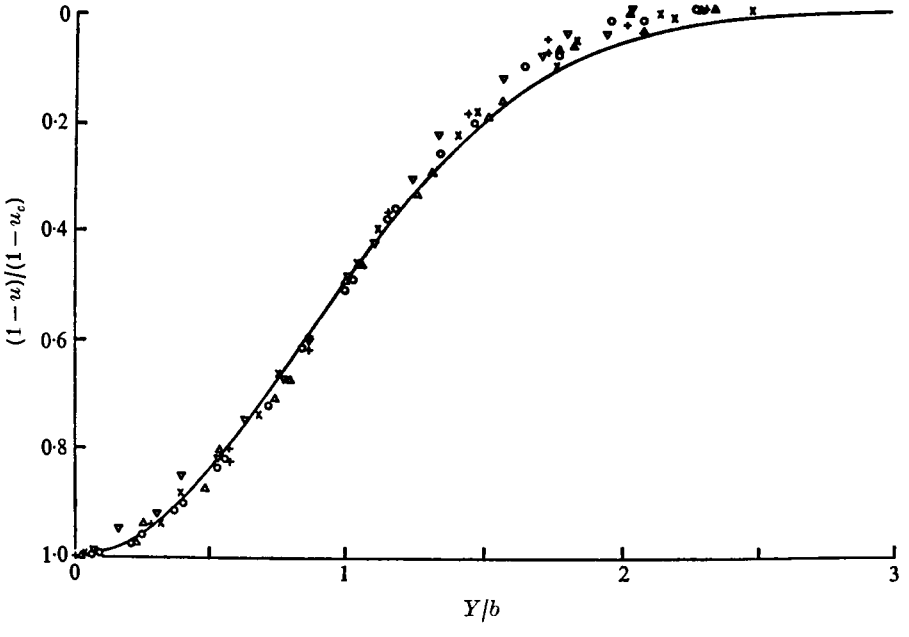

FIGURE 5. Non-dimensional velocity defect *vs.* normalized radial co-ordinate at locations further downstream. ×, $x = 1$; ○, $x = 2$; +, $x = 3$; △, $x = 4$; ▽, $x = 5$; ——, equation (27).

For our present experiment we find

$$U_0 l/\nu = 3{\cdot}27 \times 10^4 \quad \text{and} \quad [\partial(U/U_0)/\partial(Y/l)]_{x,\,y=0} = 28{\cdot}8,$$

hence

$$u_c = 0{\cdot}534 x^{\frac{1}{3}}. \tag{24}$$

This relation is plotted as a straight line in figure 3. Although the nearly perfect agreement of (24) with the present experimental results indicates that the essential process is axisymmetric radial diffusion, the degree of agreement and the longitudinal extent of validity are far better than expected and must have resulted from the particular velocity profile at the trailing tip. Unlike the flat-plate boundary layer, the boundary-layer development over an axisymmetric body depends upon its shape and probably on the Reynolds number also. Therefore (24) is unlikely to be universal.

If the same analysis is applied to the two-dimensional wake behind a flat plate, we obtain

$$u_c = (3c^2 x)^{\frac{1}{3}}, \tag{25}$$

in which c is now the Blasius constant 0·332. Hence

$$u_c = 0{\cdot}692 x^{\frac{1}{3}} \tag{26}$$

should be a universal formula independent of the Reynolds number. Equation (26), however, underestimates Goldstein's result (1930) by 10%, probably owing to a stronger convective effect, i.e. the negative displacement effect by the acceleration near the plane of symmetry, which is completely neglected in the present approximation.

Now let us turn our attention to the velocity-defect profile that is conventionally used to correlate the velocity distributions in wakes. Plotted in figure 4 is the non-dimensional velocity defect $(1-u)/(1-u_c)$ *vs.* the radial co-ordinate normalized by the half-wake radius b, which is the radial distance where the velocity defect is $\frac{1}{2}$. It is indeed amazing that the velocity-defect profile acquires an approximate similarity quite promptly, within one-tenth of a body length behind the trailing tip. The velocity-defect profiles for the range further downstream are shown in figure 5. Although it is not quite accurate, particularly near the outer boundary of the wake, the similarity profile may be approximated by

$$(1-u)/(1-u_c) = \exp[-(Y/b)^2 \ln 2]. \tag{27}$$

Because of the formal mathematical similarity, one might hastily conclude that the asymptotic similarity solution (6) has been promptly reached and that the remaining problem merely amounts to locating an artificial origin of the x co-ordinate so as to correlate other wake characteristics. But this is not the case. For example, the half-wake radius increases almost linearly after a sudden initial jump (figure 6) throughout the entire test length of the present experiment, whereas the asymptotic far-wake solution predicts a $\frac{1}{2}$-power increase.

The rest of the paper is concerned primarily with the proper characterization of the wake development.

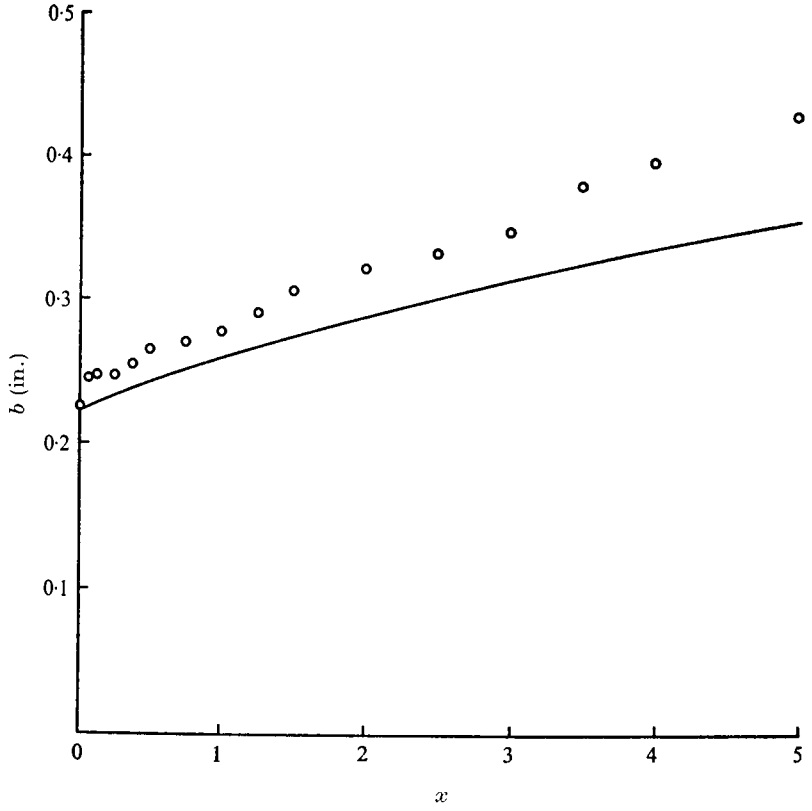

FIGURE 6. Half-wake radius *vs.* downstream distance. ○, present experimental data; ———, equation (30) with equations (33) and (38).

With the similarity profile (27), the momentum area becomes

$$\Theta = \frac{b^2}{2\ln 2}(1-u_c^2), \tag{28}$$

which in turn is related to the drag coefficient C_D ($= D/\frac{1}{2}\rho U_0^2 \pi(\frac{1}{2}d)^2$) by

$$\Theta = \tfrac{1}{8}C_D \pi d^2. \tag{29}$$

It is essential to stress that, unlike the far-wake asymptotic analysis, $1-u$ is not neglected in comparison with unity in obtaining (28). The half-wake radius b is then given by

$$b^2 = \tfrac{1}{4}\ln 2 C_D d^2/(1-u_c^2) \tag{30}$$

and the displacement area Δ by

$$\Delta = \tfrac{1}{4}\pi C_D d^2/(1+u_c). \tag{31}$$

As before, we may now substitute u as given by (27) into (1) and obtain the condition on the wake axis:

$$u_c \frac{du_c}{dx} = \frac{\nu l}{U_0 b^2}(1-u_c)\,4\ln 2. \tag{32}$$

Substitution of (30) into (32) and an integration result in

$$x = \frac{C_D}{64}\frac{U_0 d}{\nu}\frac{d}{l}\left[\frac{2}{1-u_c} + \ln\frac{1-u_c}{1+u_c} - 2\right], \tag{33}$$

in which the integration constant is determined by the condition $u_c = 0$ at $x = 0$. Thus b and Δ are related to x through u_c, whereas Θ should remain constant.

These relations have correct asymptotic behaviour far downstream. In the limit $u_c \to 1$, equation (33) becomes

$$1 - u_c \approx \frac{C_D}{32}\frac{U_0 d}{\nu}\frac{d}{l}\frac{1}{x} = \frac{A}{x}, \tag{34}$$

in agreement with (6). Equation (30) will tend to

$$b^2 \approx \frac{\ln 2}{8}\frac{C_D d^2}{A}x = \frac{4\nu X}{U_0}\ln 2, \tag{35}$$

in accord with (7). It is obvious from (29) and (31) that Δ will be identical with Θ in the far-wake limit.

In the near-wake limit $u_c \to 0$, however, (33) becomes

$$u_c^2 \approx \frac{32}{C_D}\frac{\nu}{U_0 d}\frac{l}{d}x \tag{36}$$

and does not comply with the proper $\frac{1}{3}$-power property as expressed by (23), simply reflecting the fact that the similarity profile (27) is not established immediately. Incidentally, the half-wake radius may also be calculated using the hyperbolic profile (21) exclusively, resulting in

$$b = \frac{l}{2c}\left(\frac{\nu}{U_0 l}\right)^{\frac{1}{2}}[(1-u_c)(1+3u_c)]^{\frac{1}{2}}. \tag{37}$$

This relationship explains quite well the initial behaviour of b, which first jumps almost instantaneously from the boundary-layer value and then remains nearly constant before increasing steadily. Equation (37) indicates, however, that b decreases for u_c larger than $\frac{1}{3}$, which corresponds to $x = 0{\cdot}243$. Hence it fails to represent the experimental values of b properly beyond this limit, probably because the assumed hyperbolic profile does not adequately describe the true velocity profile away from the near-axis region, particularly for larger values of u_c.

The momentum area and the displacement area were calculated from the measured velocity profiles and are plotted in figure 7. From the average value of the momentum area, we find

$$C_D = 0{\cdot}553. \tag{38}$$

With this drag coefficient the relation between the centre-line velocity defect $1-u_c$ and the downstream distance in body lengths x is determined by (33). This relationship can then be used to relate the half-wake radius b and the displacement area Δ to x.

General features of the dependence of $1-u_c$ on x are well represented by the present analysis as shown in figure 8. Although the present measurements extend

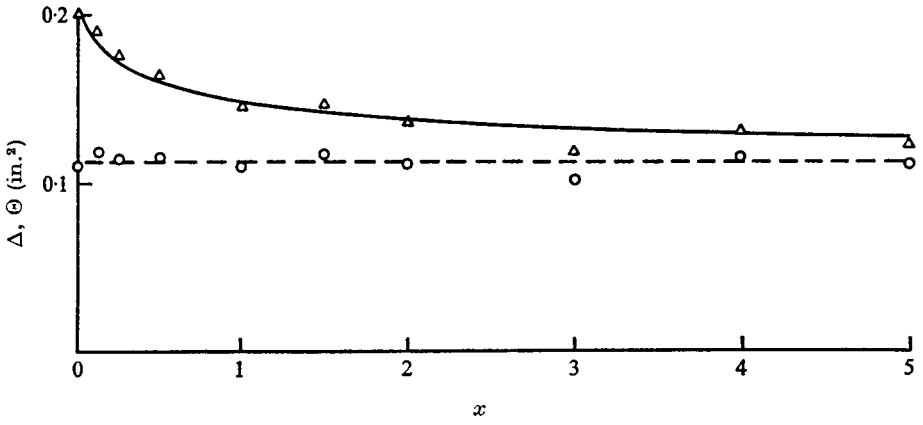

FIGURE 7. Variation of displacement area (triangles) and momentum area (circles) with downstream distance. — —, average momentum area = 0·112 in.²; ———, equation (31) with equations (33) and (38).

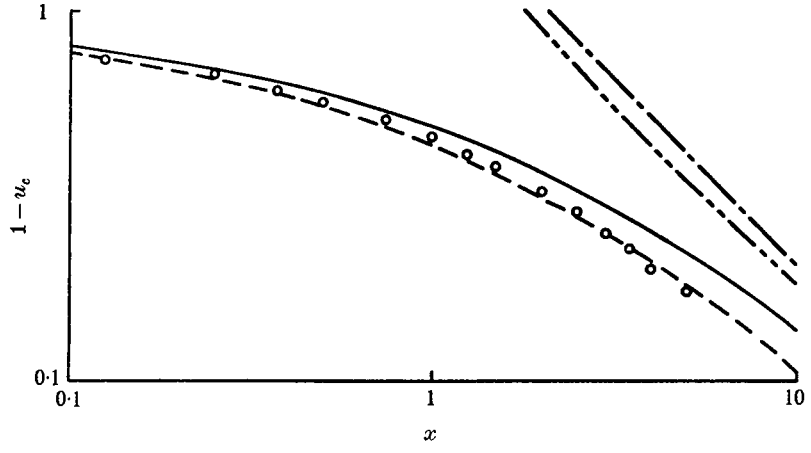

FIGURE 8. Centre-line velocity defect *vs.* downstream distance. ———, equation (33) with $C_D = 0{\cdot}553$; — —, equation (33) with $C_D = 0{\cdot}395$; — · —, asymptotic solution (6) with $A = 2{\cdot}06$; — · · —, second approximation (20) with $C = 0$.

as far downstream as five body lengths, $1 - u_c$ is still far from reaching its asymptotic form. No simple shift of co-ordinate origin makes either the experimental data or (33) match with the asymptotic solution. By a shift of co-ordinate origin, it is possible to make $1 - u_c$ inversely proportional to the adjusted x co-ordinate but the proportionality factor cannot be A. Moreover, the same amount of origin adjustment cannot even make the half-wake radius b proportional to $x^{\frac{1}{2}}$.

It is, therefore, needless to repeat that the analysis presented here differs from the asymptotic solution in the retention of $1 - u$ compared with unity. The second approximation (20) is also shown in figure 8 (with $A = 2{\cdot}06$ and $C = 0$) to demonstrate that it does not give much improvement over the first approximation. Nevertheless, (33) overestimates x appreciably for given u_c. In fact, if C_D were reduced by 40 %, i.e. $C_D = 0{\cdot}395$, agreement with the experimental values

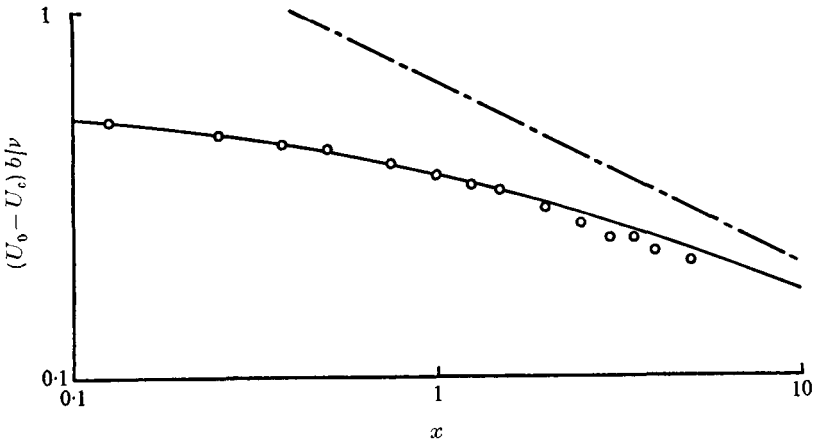

FIGURE 9. Wake Reynolds number *vs.* downstream distance. ○, present experimental data; ———, equation (39); — — —, asymptotic solution (41).

would become almost perfect, but we can find no justification for such an adjustment. The disagreement cannot be accounted for by asymmetry in the wake. At the time of writing we do not know of legitimate means of obtaining agreement.

In figure 6, b is cross-plotted against x. The present analysis describes its general behaviour quite well except for the initial jump. The analysis underestimates the experimental values owing to the difference between the experimentally obtained velocity profile and the similarity profile, the former being narrower than the latter near the outer boundary. Whereas b is obtained from the experimental profile as the radius where the velocity defect is half the centre-line velocity defect, the analysis determines b by matching the integrated momentum Θ. Therefore, the discrepancy shown in figure 6 can be easily reconciled by redefining b by use of (28) and measured Θ and u_c. The reduction of C_D by 40 %, which made the analytical relationship between $1-u_c$ and x agree with the experimental data, decreases the prediction of b to unacceptably low values and hence is not a consistent procedure.

Figure 7 shows excellent agreement between the experimental values of Δ and the analysis. This figure also demonstrates that substantial differences between Δ and Θ still exist and that approaching the asymptotic similarity solution is indeed an extremely slow process. The strength of this particular figure in making such a conclusion is that, whereas one may still try to reconcile the differences between the experimental and the asymptotic values in other figures by a shift of the virtual origin of x, such an adjustment is of no avail with the differences between Δ and Θ.

Finally, the wake Reynolds number defined by $(U_0-U_c)b/\nu$ is plotted in figure 9 against x. According to the semi-empirical formulation developed here, it is given by

$$\frac{(U_0-U_c)b}{\nu} = \frac{1}{2}\frac{U_0 d}{\nu}\left[C_D\frac{1-u_c}{1+u_c}\ln 2\right]^{\frac{1}{2}}, \tag{39}$$

which agrees quite well with the experiment. Equation (3) has the following far-wake asymptotic form for $u_c \to 1$:

$$\frac{(U_0 - U_c)b}{\nu} \approx \tfrac{1}{16} C_D \left(\frac{U_0 d}{\nu}\right)^{\frac{3}{2}} \left[\frac{d}{l}\frac{1}{x}\ln 2\right]^{\frac{1}{2}}, \tag{40}$$

or with the present experimental values,

$$(U_0 - U_c)\, b/\nu \approx 630 x^{-\frac{1}{2}}. \tag{41}$$

It is seen that the wake Reynolds number indeed decreases with downstream distance, but at a rate much slower than the asymptotic solution, and has not reached the asymptotic state.

5. Conclusion

The mean-velocity profiles in a steady laminar wake behind a slender axisymmetric body were measured at the body-diameter Reynolds number 2000. The centre-line velocity increased with downstream distance to the power $\frac{1}{3}$, this trend persisting for as long a distance as two body lengths. The velocity profiles acquired an approximate similarity quite promptly, within one-tenth of a body length. The experimental results and the semi-empirical analysis based upon approximate similarity, in which the nonlinear term is retained, clearly indicated that the flow development is an extremely slow process, requiring a far longer distance than the five body lengths available in the test section to reach the asymptotic similarity condition.

The work is part of the continuing research supported by the National Science Foundation under grants GK-20409 and ENG 74-21490. The authors are grateful to their colleagues at Princeton University for their fraternal encouragement, if nothing else, and particularly to Harvey Lam for his always inspiring discussions.

REFERENCES

BAILY, D. A. 1972 M.S.E. thesis, Department of Aerospace and Mechanical Sciences, Princeton University.

BERGER, S. A. 1968 *J. Math. & Phys.* **47**, 292.

GLAUERT, M. B. & LIGHTHILL, M. J. 1955 *Proc. Roy. Soc.* A **230**, 188.

GOLDSTEIN, S. 1930 *Proc. Camb. Phil. Soc.* **26**, 1.

GOLDSTEIN, S. 1933 *Proc. Roy. Soc.* A **142**, 545.

MATTINGLY, G. E. & CRIMINALE, W. 1972 *J. Fluid Mech.* **51**, 233.

MORROW, T. B. & KLINE, S. J. 1971 *Dept. Mech. Engng, Stanford Univ. Rep.* MD-25.

PATEL, V. C., NAKAYAMA, A. & DAMIAN, R. 1974 *J. Fluid Mech.* **63**, 345.

PETERSON, L. F. 1975 Ph.D. thesis, Department of Aerospace and Mechanical Sciences, Princeton University.

ROSENHEAD, L. (ed.) 1963 *Laminar Boundary Layers.* Oxford University Press.

SATO, H. & KURIKI, K. 1961 *J. Fluid Mech.* **11**, 321.

STEWARTSON, K. 1957 *J. Math. & Phys.* **36**, 173.

TOLLMIEN, W. 1931 *Handbuch d. Exp. Phys.* IV-1. Leipzig: Akademie Verlag.

VIVIAND, H. & BERGER, S. A. 1965 *A.I.A.A. J.* **3**, 1806.